Understanding the effects of processing conditions on the formation of lamellar gel networks using a rheological approach

Cunningham, Grace E.; Alberini, Federico; Simmons, Mark J.h.; O'sullivan, Jonathan J.

DOI:
10.1016/j.ces.2021.116752

Document Version
Peer reviewed version

Citation for published version (Harvard):
Cunningham, GE, Alberini, F, Simmons, MJH & O'sullivan, JJ 2021, 'Understanding the effects of processing conditions on the formation of lamellar gel networks using a rheological approach', *Chemical Engineering Science*, vol. 242, 116752. https://doi.org/10.1016/j.ces.2021.116752

Understanding the effects of processing conditions on the formation of lamellar gel networks using a rheological approach

Grace E. Cunningham[1,2], Federico Alberini[1], Mark J.H. Simmons[1,*], Jonathan J. O'Sullivan[2]

[1] Centre for Formulation Engineering, School of Chemical Engineering, University of Birmingham, Edgbaston, Birmingham B15 2TT, UK

[2] Unilever Research & Development, Port Sunlight Laboratory, Quarry Road East, Bebington, Wirral CH63 3JW, UK

* Corresponding author: Email address: M.J.Simmons@bham.ac.uk

ABSTRACT

Lamellar gel networks are multiphase systems which form the basis of many cosmetic and pharmaceutical cream products, thanks to their superior stability compared to typical oil-in-water emulsions, and highly desirable rheological properties inferred by the interconnected structure. There has previously been considerable interest in the formulation of lamellar gel networks, but little interest has been given to the effects of processing conditions on the formation of the desired structure, or the possibility for process optimisation through understanding power consumption. The evolution of the microstructure of an incipient lamellar gel network during processing was investigated by varying the temperature, vane speed and time using a rheometer equipped with a four-bladed vane in cup geometry. Torque and vane speed measurements were recorded at 2 Hz for the duration of the experiment, from which apparent viscosity (taken at a reference shear rate of 200 s^{-1}) and power input were calculated. Samples were then characterised by yield stress and flow curve measurements to determine the impact of processing conditions on the final product microstructure. Increasing vane speed increased the maximum apparent viscosity achieved and yield stress of the sample, and reduced

the time taken to reach the peak apparent viscosity. However, the increased power requirements from the higher vane speed were not counteracted by shorter processing times. Increasing the temperature reduced the rate of apparent viscosity increase but did not affect the yield stress of the final lamellar gel network, offering a reduction in power consumption due to a lower apparent viscosity for the majority of the process.

KEYWORDS

Lamellar structured liquids, Rheological mapping, Process development, Yield stress, Time-evolving rheology

HIGHLIGHTS

- Lamellar structured liquids were prepared using a rheometer with vane geometry.
- Effects of temperature, vane speed and time on evolving rheology investigated.
- Insight into kinetics of lamellar gel network formation.
- Yield stress of LGNs improved by reducing time and increasing vane speed.
- Power requirements increased linearly with time and vane speed.

1 INTRODUCTION

The basis of many cosmetic and pharmaceutical cream products, such as hair conditioner, facial creams, moisturisers and topical medications, is an oil-in-water emulsion, stabilised by ionic or non-ionic surfactants and long-chain fatty alcohols (FA) (Junginger, 1984). When these ingredients are combined, a multiphase colloidal structure known as a lamellar gel network (LGN) is formed. The key component of the LGN is the lamellar gel phase, L_β, which consists of hexagonally packed, solid-state amphiphilic molecules (surfactant and FA) arranged in regularly spaced, planar bilayers, swollen by interlamellar aqueous phase. The remainder of the bulk aqueous phase is in dynamic equilibrium with this interlamellar phase (Junginger, 1984). The lamellar gel phase can exist as an interconnected system of planar sheets, or spherical multilamellar vesicles (Iwata, 2017). Other oil phase ingredients, generally included in cosmetic and pharmaceutical formulations, exist as droplets surrounded by a single layer of amphiphilic molecules (Iwata, 2017).

The multiphase nature of the LGN structure imparts several properties which make it highly desirable for formulating cosmetic and pharmaceutical cream products, in terms of opaque appearance, slippery and oily texture, rheological properties, emulsion stability and delivery of active ingredients (Iwata, 2017). As the amphiphilic molecules exist in their solid-state in an LGN, when applied to the skin, this imparts an oily tactile feel. This is further enhanced by the bi-continuous arrangement of the layers, whereby a greater amount of amphiphiles have contact with the skin than in typical emulsions. The amphiphiles used in LGNs are typically water-insoluble (hence more hydrophobic than typical oil-in-water surfactants). Therefore, the amphiphiles can be used to deliver cosmetic benefit in rinse-off cosmetic products (Iwata & Aramaki, 2003).

Perhaps the most important aspect of the lamellar gel network is the bulk rheological properties it imparts. The system is a highly viscous, shear-thinning material which possesses a high yield stress due to the interconnected lamellar gel phase (Datta, et al., 2020). The rheology of the system is highly dependent on the type, concentration and ratio of FA and surfactant used (Nakarapanich, et al., 2001), which has been the subject of considerable research effort (Awad, *et al.,* 2011; Fukushima & Yamaguchi, 1983; Iwata & Aramaki, 2003; Nakarapanich, *et al.,* 2001)

However, the method of preparation as well as the formulation has considerable impact on the final structure and resultant rheological properties (Colafemmina*, et al.,* 2020; Eccelston, 1997).

In typical colloidal systems, the surfactant concentration is kept below the solubility limit to prevent precipitation, and the intended storage and usage temperature of the product is higher than the Krafft point to allow a higher concentration of surfactant than the critical micelle concentration in the system (Nakama, 2017). However, a lamellar gel phase, L_β, is formed when the total surfactant concentration is above the solubility limit and the system is below the Kraftt point, (Davies & Amin, 2020). Lamellar gel networks can therefore be prepared by heating the ternary phase ingredients (FA, surfactant and water) to a temperature above the melting point of the FA, homogenising, and cooling to room temperature (Davies & Amin, 2020; Wunsch, *et al.,* 2015; Yang, 2017). When the mixture is heated to above the Krafft point, the surfactants are in a stable, spherical micellar solution. When the system is cooled to below the solubility limit, the surfactants phase separates from the solution and forms various crystalline structures dependant on the critical packing parameter, CPP, a property based on the geometry of the surfactant which determines the type of micellar aggregate formed (Nakama, 2017). When a ratio of FA and surfactant is used that gives a CPP close to 1, the molecules form lamellar bilayers, which can hold large amounts of water between them, mainly due to the repulsive forces between the layers, *i.e.,* lamellar gel phase, L_β (Fairhurst, *et al.,* 2008, Ribiero, *et al.*, 2004; Wunsch, *et al.,* 2015; Yamagata & Senna, 1999). If the system is purely cetostearyl alcohol with no additional surfactant, then the system will still form lamellar bilayers, but with much tighter packing, and only a small amount of water between layers – this is known as lamellar coagel phase, L_c. Finally, if the temperature is above the melting point of the hydrocarbon chains of the amphiphiles, the system transitions from a gel state to a lamellar liquid crystal state, where packing of the surfactants is looser and the overall behaviour of the system is more liquid like (Davies & Amin, 2020).

There are some discussions in the literature regarding the effects of thermal profile, temperatures, and shearing effects on the final properties of LGNs. Iwata suggested that, on a commercial manufacturing scale, insufficient mixing, or cooling the mixture too quickly before the

lamellar gel phase has formed (perhaps due to a high temperature gradient between the product within the vessel and the coolant in the jacket of the vessel), can lead to a higher percentage of hydrated crystals of FA which are not incorporated in to the gel phase (Iwata, 2017). This reduces stability of the gel network, and affects the shear-thinning properties, as the hydrated FA crystals are hydrogen-bonded and do not slip over each other. Fukushima and Yamaguchi, (1983), Ito *et al.,* (2011) and Partal *et al.,* (2001) found that applying increasing shear onto a lamellar structure forces the bilayers to form vesicles, as the 'infinite' sheets cannot accommodate the flow. Colafemmina *et al.,* (2020) investigated the effects of different cooling rates on the final structural and rheological properties of a LGN using rheology, small-angle X-ray scattering (SAXS) and diffusion NMR. They found that cooling the system rapidly (40°C/min) in contrast to cooling slowly (5°C/min) produced a more favourable structure and rheological properties *i.e.,* higher yield stress. However, there remains relatively little insight on the relationship between processing variables, such as: thermal profile, mixing time, mixing intensity, shear rate, and scale of manufacture on the physicochemical and rheological properties of the final LGN and this requires further investigation (Ballmann & Mueller, 2008; Colafemmina, *et al.,* 2020; Davies & Amin, 2020; Ito, *et al*., 2011; Yang, 2017).

Whilst research publications regarding manufacturing of lamellar gel networks is limited, there are some patent applications from several global personal care and cosmetic companies (Unilever (EP2877144 A1), Procter & Gamble (US2009324527 A1, EP2460508 A1), L'Oreal (US5246693)) disclosing manufacturing methods and process parameters such as: processing temperatures and temperature profiles, suitable fatty alcohol and surfactant combinations, order of addition of ingredients, mixing intensity, energy input, suitable equipment. In summary, the oil-phase ingredients (i.e., fatty alcohol and surfactant) are prepared to a temperature above the melting point of the components (typically ~85°C) and combined with the aqueous phase which is prepared at a lower temperature to ensure that when combined, the temperature of the mixture is 57-70°C. After mixing, the product is cooled either via jacket cooling or addition of ambient materials (Flanagan, 2013; Grollier & Richoux, 1993; Venkateswaran, *et al*., 2009; Zhong & Toshiyuki, 2009).

The formation of a LGN inherently involves a large increase in viscosity of the system as the microstructure is generated (Iwata & Aramaki, 2013). It would therefore be highly beneficial to measure the rheology of the incipient LGN in situ to investigate the effects of varying different process conditions from which the structure can be inferred. This can be achieved by using a *mixing rheometry approach*, in which torque requirements are measured throughout the process, and an analytical approach such as the Couette analogy, or an empirical method such as the Metzner-Otto approach which are used to convert torque-speed data to apparent viscosity measurements (Bousmina, *et al.,* 1999; Metzner & Otto, 1957). By utilising a rheometer with a cup geometry to represent the manufacturing vessel, albeit at a much smaller scale, this is easily achieved. Different geometries such as helical ribbons, anchors, paddles and vanes have been used to follow the apparent viscosity of a system as it evolves, and to measure power consumption (Ait-Kadi, et al., 2002). Franco *et al.* used a torque measuring device paired with an anchor agitator and high shear device to follow the manufacture of lubricating greases and characterise the power consumption of each stage, using the Metzner-Otto approach (Franco, et al., 2005). Chavez-Montes *et al.,* (2003) and Choplin *et al.* (1998) both used a rheometer with adapted mixing geometries to investigate the changing rheological properties of ice-cream and cosmetic lotions, respectively. A similar approach was used by Gaiani et al. to follow the dissolution behaviour of phosphocaseinate at different temperatures and times, using a vane attachment. The viscosity profile was matched to the measured particle size of the phosphocaseinate to determine the time taken for different phases of the dissolution process *i.e.,* wetting, swelling and dissolution (Gaini, et al., 2006).

The work presented in this paper describes how the rheological properties of an incipient LGN evolve as a function of time when different processing conditions, namely vane speed, processing time, and processing temperature, are employed. A ternary system of cetostearyl alcohol (FA) (7.06 wt%), behentriominum surfactant (BTAC) (2.35 wt%) and water was chosen to study. Cetostearyl alcohol is a popular commercially available fatty alcohol used in the formulation of many personal care and cosmetic products, and BTAC is a quaternary ammonium salt most commonly used in the formulation of hair conditioners. This formulation has been studied elsewhere, is known to

generate a lamellar structure, and is representative of the rheology of a fully formulated cosmetic or personal cream product (Davies & Amin, 2020). The relationship between the processing conditions and the final product quality will be explored, in terms of final rheological properties of the product, and process optimisation, in terms of power consumption.

2 MATERIALS AND METHODS

2.1 Materials

The fatty alcohol (FA) used as part of this study was a commercially available blend of cetyl alcohol (30 wt. %) and stearyl alcohol (70 wt. %) (cetostearyl alcohol) sourced from Godrej Industries (India). The surfactant used was behentrimonium trimethyl ammonium chloride (BTAC), supplied by Clairant International Ltd. (Germany). This surfactant is provided at 70 wt. % purity, where the remaining 30 wt. % is comprised of dipropyl glycol, which acts as a processing aid. Glycerine (Palmera G995E; >99.5% purity; supplied by KLK Oleo) was used for the purpose of calibrating the vane geometry (viscosity @ 25°C: 0.95 Pa s). Distilled water was used for all experiments.

2.2 Preparation of lamellar gel network (LGN) samples

A Discovery HR-III stress-controlled rheometer (TA Instruments, UK) with a four-bladed vane spindle geometry was used for the preparation of the LGNs (dimensions of the geometry are shown in Figure 1).

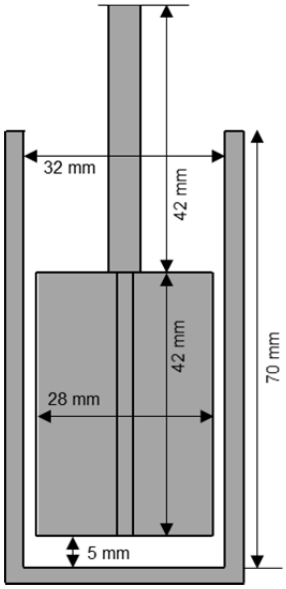

Figure 1. Dimensions of rheometer geometry with four-bladed vane attachment and associated cup

168

169 The samples were prepared and processed in the rheometer in the following stages.

170 *Preparation stage.* 7.06 wt. % (of total formulation) of FA and 90.59 wt. % of distilled water was
171 added to the rheometer cup with a targeted total batch size of 34g. The cup was installed in the
172 rheometer and the mixture heated to a temperature of 70°C, with the vane at a shear rate of 200 s^{-1}.
173 Once at 70°C, the sample was stirred for 5 min, and then cooled to the temperature required for the
174 structuring stage.

175 *Structuring stage*. Once at the appropriate defined temperature, 2.35 wt. % of BTAC was added to
176 the rheometer cup and stirred for the desired time and at the defined vane speed; values of these
177 parameters are given in Table 1. The reference conditions for this study were a temperature of 60°C,
178 shear rate of 200 s^{-1}, and time of 30 min.

179 *Cooling stage*. After the structuring stage, the sample was cooled at a rate of 5 °C min^{-1} to a final
180 target temperature of 30°C whilst continuing to mix at a shear rate of 200 s^{-1}.

181

Table 1. Investigated variable of vane speed, temperature, and time for the structuring stage of LGN preparation

LGN	LGN_{ref}	$LGN_{T=67°C}$	$LGN_{\dot{\gamma}=400}$	$LGN_{t=20}$	$LGN_{T=63°C}$	$LGN_{T=57°C}$	$LGN_{\dot{\gamma}=600}$	$LGN_{t=40}$	$LGN_{\dot{\gamma}=400;t=20}$	$LGN_{t=10}$	$LGN_{\dot{\gamma}=600;t=10}$	$LGN_{\dot{\gamma}=50}$
Vane shear rate (s^{-1})	200	200	400	200	200	200	600	200	400	200	600	50
Temperature (°C)	60	67	60	60	63	57	60	60	60	60	60	60
Time (minutes)	30	30	30	20	30	30	30	40	20	10	10	30

2.3 Calibration of vane geometry using Couette analogy and Metzner-Otto correlation

The vane geometry (*cf.*, Figure 1) used in this work is a commercially available attachment for the DHR-3 rheometer (TA Instruments, UK), thus apparent viscosity can be read directly from the rheometer software and does not need to be calculated from torque-speed data (Trios, TA instruments, UK). However, it was decided to calculate the stress and strain constants via the Couette analogy and Metzner-Otto concept for reference purposes, and in order to utilise the Metzner-Otto concept for power consumption calculations (Choplin & Marchal, 2010; Metzner & Otto, 1957). The shear stress constant (K_τ) and the shear rate constant ($K_{\dot{\gamma}}$) relate torque and rotational speed measurements to stress and shear rate as shown below:

$$\tau = K_\tau T \qquad (1)$$

$$\dot{\gamma} = K_{\dot{\gamma}} N \qquad (2)$$

Where τ is shear stress (Pa), $\dot{\gamma}$ is shear rate (s^{-1}), T is torque (N m), and N is rotational speed (rps).

The constant, $K_{\dot{\gamma}}$, which relates shear rate to rotational speed is also known as the Metzner-Otto constant (Metzner & Otto, 1957). Metzner-Otto theorised that for non-Newtonian fluids in the laminar regime, there exists an average shear rate from which the apparent viscosity can be determined. The aim of the Couette analogy is to determine the equivalent dimensions of a Couette cylinder for a non-conventional geometry which provide the same torque measurement at the same rotational speed (Ait-

Kadi, et al., 2002). Once the equivalent internal radius of the Couette cylinder has been determined analytically, the shear stress and shear rate can be calculated based on the rheological behaviour of the fluid (most commonly applied to power-law fluids). The final rheological characteristics of a LGN can be described using a power law model (Ahmadi, et al., 2020):

$$\eta = K\dot{\gamma}^{n-1} \quad (3)$$

Where η is the apparent viscosity (Pa s), $\dot{\gamma}$ is the shear rate (s^{-1}), and K and n are the consistency (Pa s^n) and flow (-) indices, respectively. The Couette analogy approach described by Ait-Kadi *et al.* (2002) has been utilised in this work to determine the shear stress constant (K_τ) and the shear rate constant ($K_{\dot{\gamma}}$) by calibration with a fluid with known power law characteristics; in this case, glycerine (>99.5% purity), a Newtonian fluid, where n=1. The values calculated for the stress and strain constants are given below (Table 2).

Table 2. Stress constant and strain constant calculate from data, Couette analogy and Metzner-Otto concept

Constant	Calculated from rheometer data for non-Newtonian fluid	Couette analogy	Metzner-Otto
Kτ	17867	16141	N/A
Kγ	76.7	69.1	76.0

The stress and strain constant values calculated using the different methods are in satisfactory agreeance. **Error! Reference source not found.** shows a flow curve for an example lamellar gel network measured using both the vane geometry and cross-hatched parallel plates, which are the conventional geometry used for measuring rheology of lamellar gel networks. The similarity of the flow curves measured using the two different geometries further proves that the stress and strain constants for the vane are accurate.

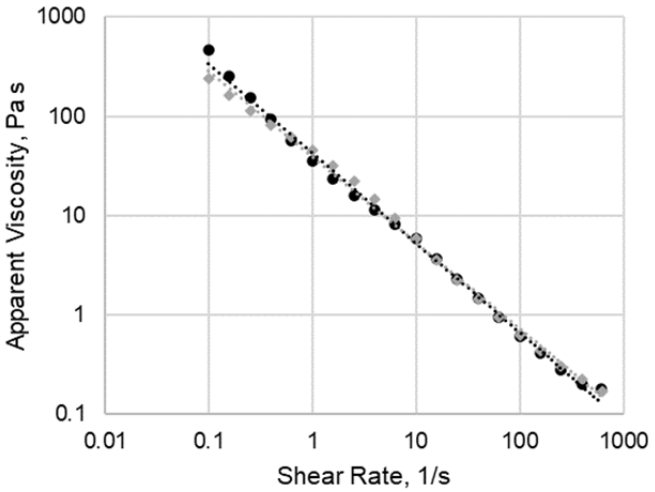

Figure 2. Flow curve of LGN_{ref} measured using vane geometry and cross-hatched parallel plates (grey diamond = vane, black circle = cross-hatched parallel plates)

218

219 *2.4 Power consumption determination*

220 By applying the Metzner-Otto concept and assuming instantaneous torque measurement,
221 instantaneous power consumption can easily be calculated using Equation 4 (W; Watts). From a plot
222 of power *vs.* time, it is then possible to calculate the energy input for the process through integration
223 of the area under the curve (Franco, et al., 2005). This has been done to calculate the energy input
224 required to achieve the maximum viscosity, as well as for the entire process.

$$\dot{W} = 2\pi N(M - M_0) \quad (4)$$

$$\dot{W} = \frac{2\pi N}{t}\int_0^t (M - M_0)dt \quad (5)$$

225

226 Where: $\dot{W}$ is power consumption (W), M is the torque value with sample (N.m), M_o is the torque value
227 without sample (N.m), and N is rotational speed (RPS), t is time (s).

228 *2.5 Corrective factor to compare samples prepared at different shear rates*

229 For LGNs prepared at different rotational speeds, a corrective factor has been applied to data to enable
230 direct comparison between samples, taking in to account the shear-thinning behaviour of the system.

Torque-speed measurements were taken for a reference Newtonian fluid (glycerine at 25°C) and the instantaneous power consumption calculated using the method described previously. Knowing the viscosity of the Newtonian system, and the power consumption for Newtonian and non-Newtonian fluid, the apparent viscosity of the non-Newtonian fluid (η; Pa s) can be determined from Equation 6.

$$W_{NN}\mu = W_N\eta \quad (6)$$

Where M is the torque value with sample (N m), M_o is the torque value with no sample (N m), W_N and W_{NN} are the power consumption for the Newtonian and non-Newtonian fluid, respectively (Franco, et al., 2005).

To estimate the apparent viscosity at the reference shear rate of 200 s^{-1} instead, N can be taken as the equivalent reference vane speed (2.61 rps) in Equation 6. This provides an insight in the apparent viscosity of the system at the reference shear rate so that it is possible to determine the effects of varying vane speed, as well as directly comparing the viscosity across samples prepared at different mixing speeds.

2.6 Rheological characterisation of LGN samples

Characterisation of all samples was carried out using the Discovery DHR-3 rheometer (TA instruments) equipped with cross-hatched parallel plates to minimise slip. All measurements were carried out at 25°C on samples aged for at least 24 h. The yield stress was measured using an oscillation amplitude sweep method, 24 h after preparation. Amplitude sweep measurements were carried out at a frequency of 0.1 Hz, and a strain of 1 – 2,000%. The yield stress was determined from a plot of storage modulus (*G'*) against oscillation stress; taken as the stress value which corresponds to the onset of the loss modulus (Davies & Amin, 2020). Flow curves of the samples were obtained using a rotational shear rate sweep from 0.1 – 1,000 s^{-1}. Flow curve data was fitted to a power-law model in the shear rate range 10 – 250 s^{-1}.

2.7 *Statistical analysis*

All samples were prepared in triplicate, and an average of the viscosity profile is presented in this study. Standard deviation of the maximum viscosity value and final viscosity value for samples were calculated to investigate replicability. The average standard deviation for the maximum viscosity value was 5.24% and for the final viscosity value was 5.89%. Yield stress measurements were also completed in triplicate and an average and standard deviation is presented in the text. Student's t-test ($\alpha = 0.05$) were utilised to compare samples against the reference conditions.

3 RESULTS AND DISCUSSION

3.1 *Analysis of effects of process conditions of formation of LGNs*

3.1.1 *Analysis of rheological mapping profile for the preparation of LGN at reference conditions*

An example of an apparent viscosity-time plot for LGN_{ref} is shown in **Error! Reference source not found.**, with key parts of the curve labelled and attributed to different parts of the process to aid in

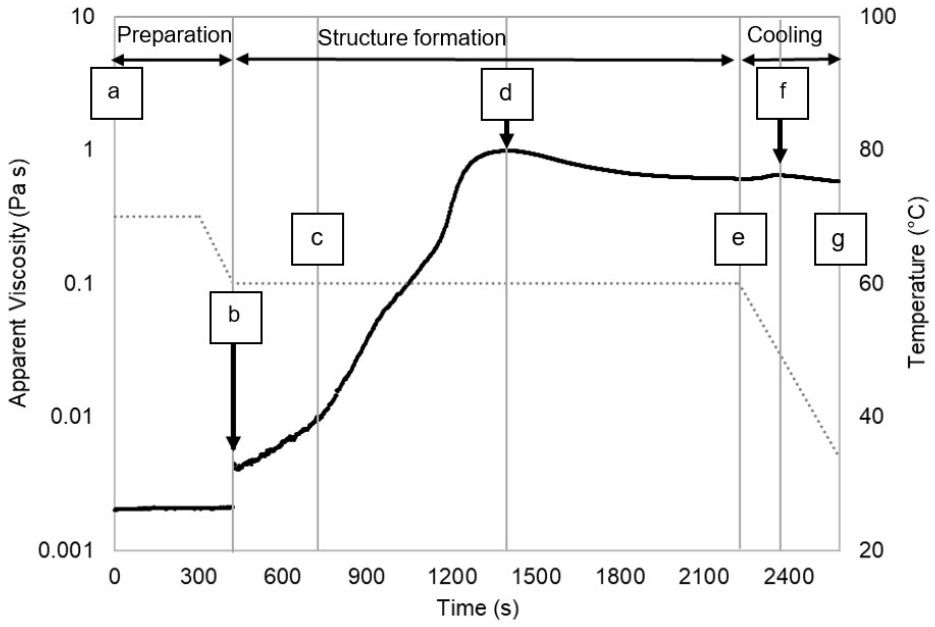

Figure 3. Viscosity-time profile of lamellar structured liquid (LGNref) prepared at reference conditions (structuring stage: temperature 60°C, vane speed 200/s, time 30 minutes)

comparison with other LGNs prepared at different conditions.

The process starts at point *a* (t = 0s), where water and FA is being agitated at 200 s^{-1}. The temperature is at 70°C for the first 300 s, and then reduced to 60°C, the temperature being investigated for the structuring stage. During the preparation stage, the mixture is an unstable emulsion of FA liquid crystals and water (Yamagata & Senna, 1999). The viscosity remains constant as both the microstructure and the processing conditions are in steady state. At point *b* (t = 420 s), BTAC is introduced into the cup. There is an initial jump in the viscosity due to solid particulates having been introduced. The figure then shows an increase in viscosity from *b* to *c,* where the BTAC is melting and beginning to combine with the FA and water, which lasts for ~300 s. From *c* to *d* the viscosity continues to increase to the maximum value at *d* (0.99 Pa s, 1340 s). Between these stages a plateau in the apparent viscosity can be seen (t = 950 s to t = 1150 s). Work by Gentile *et al.* (2012; 2014) on shear-induced transitions from lamellar sheets to multilamellar vesicles (MLVs) in single surfactant aqueous systems ($C_{12}E_3/D_2O$) showed a similar plateau at an intermediate time when the system was subjected to much lower shear rates. This was attributed through rheo-SALS and other techniques to be caused by an intermediate aggregate structure being formed. A similar transition could be occurring in this system and this idea is supported by the presence of MLVs in the final products (Gentile, *et al.,* 2012; Gentile, *et al.,* 2014). The overall viscosity gradient from *b* to *d* is 6.1 x 10^{-2} Pa s min^{-1}. After the peak at *d,* the viscosity then slightly reduces and levels out around t = 2000 s at a viscosity value of 0.61 Pa s. The cooling stage commences at *e* (t = 2220 s). A lower second peak in viscosity is seen at *f* (0.64 Pa s) at a temperature ~51°C, before the viscosity continues to slightly decrease to a final value of 0.58 Pa s at *g*. The second peak in viscosity could correlate to the transition of the lamellar liquid crystal structure to a lamellar gel phase, where the hydrocarbon chains reach a temperature below their melting point, the surfactant packing becomes more ordered, and more swelling occurs. Ribiero *et al.* (2004), performed DSC on different semisolid O/W creams containing cetyl alcohol and non-ionic surfactant, and observed a broad endotherm around 55°C, which they constituted towards the transition to and swelling of the lamellar gel phase.

3.1.2 *Effects of temperature on the formation of LGNs*

The effect of processing temperature on the viscosity of the incipient LGN was explored by varying the temperature during the structuring stage and maintaining the time and vane speed at the reference conditions of 30 min and 200 s^{-1}, respectively. Temperatures of 57°C, 60°C, 63°C and 67°C were

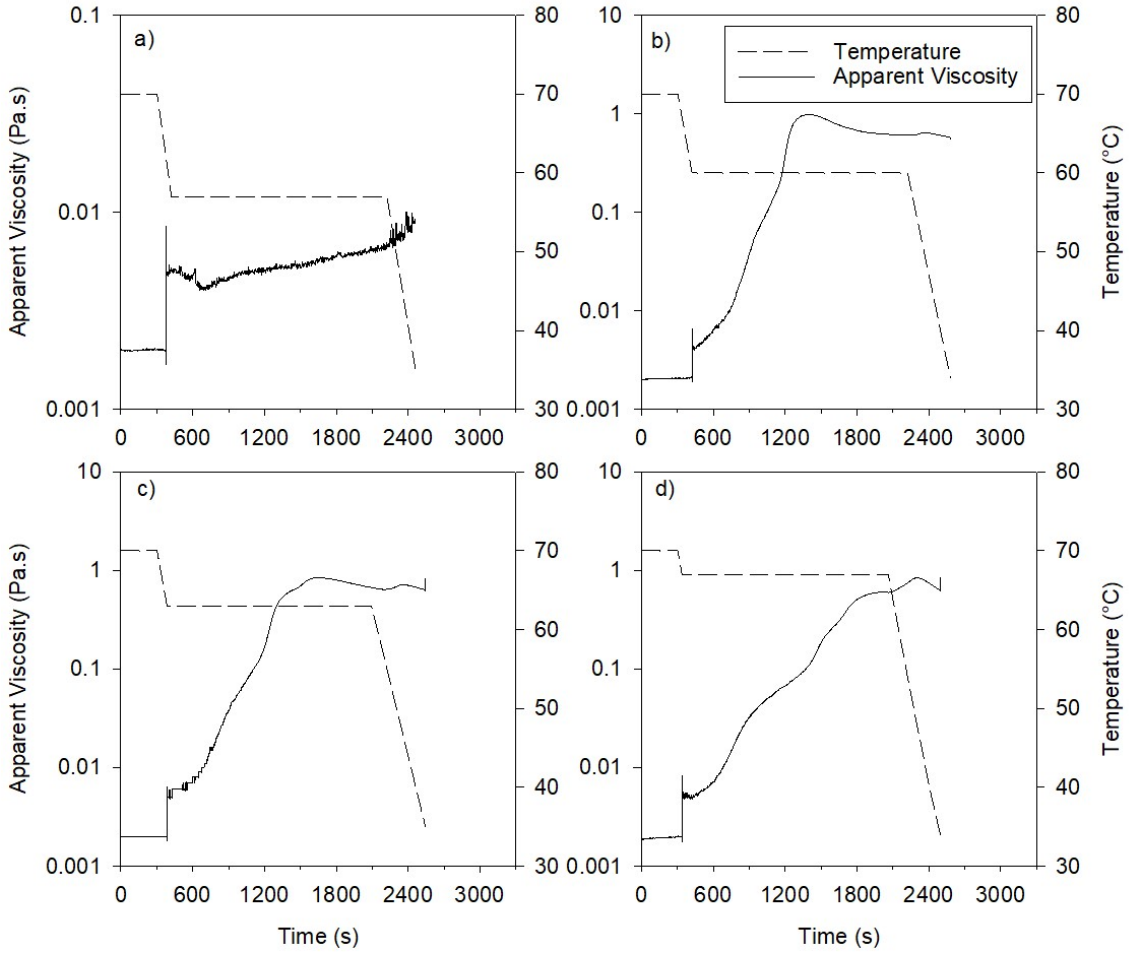

Figure 4. Apparent viscosity-time plots for LGNs prepared at different structuring stage temperatures. a) $LGN_{T=57}$ b) LGN_{ref} c)$LGN_{T=63}$ d)$LGN_{T=67}$; (dashed line = temperature profile; solid line = apparent viscosity)

investigated. The viscosity profiles for these samples are given in Figure 4.

For a processing temperature of 57°C (Fig. 4a), the viscosity of the system does not increase significantly in comparison to the other investigated temperatures. This behaviour was ascribed to insufficient temperature to melt the BTAC in solution (melting point = 52-64°C; dependent on purity)

(Clairant Corporation, 2018), thus the required emulsification with the FA did not occur and the lamellar structure was not formed. This was evident due to the inhomogeneous nature of the prepared sample (*i.e.*, presence of not melted solid particulates) which did not possess sufficient structure for yield stress characterisation. Fig. 4b shows the viscosity profile for LGN_{ref}, which was prepared at a processing temperature of 60°C. This viscosity profile is previously discussed in Section 3.1. (*cf.,* Fig. 3). A comparable trend was observed for $LGN_{T=63°C}$ (Fig. 4c) in terms of viscosity profile, where certain distinct differences were exhibited. The viscosity gradient from *b* to *d* was less steep for $LGN_{T=63°C}$ (4.2×10^{-2} Pa s min^{-1}) than the reference conditions (6.1×10^{-2} Pa s min^{-1}), with the peak viscosity at *d* (0.86 Pa s) occurring at 1650s, 250s later than for LGN_{ref}. The viscosity profile for $LGN_{T=67°C}$ (Fig. 4d) shows a slightly different trend to LGN_{ref} and $LGN_{T=63°C}$. The peak viscosity (0.79 Pa s) occurs considerably later for $LGN_{T=67°C}$ and occurs during the cooling stage rather than the structuring stage (~ 2380s) when the temperature has reduced to 47.5°C. This behaviour is thought to be associated with a combination of elevated temperatures reducing the magnitude of the viscosity response, and that lower processing temperatures form LGNs at a faster rate as seen through the rate of change of viscosity in comparison to the other investigated temperatures (Fig. 4b, c). The peak in viscosity at around 50°C for $LGN_{T=67°C}$ again corresponds to the temperature seen for the transition to a swollen gel phase from the lamellar liquid crystal phase (Ribiero, *et al*., 2004; Wunsch, *et al.,* 2015). Nevertheless, no significant differences ($p > 0.05$) were seen for the final viscosity values (0.59 ± 0.03 Pa s) and yield stress measurements (105 ± 3 Pa) across the samples prepared at 60 - 67°C. However, when the temperature was increased to 67°C, there was a slight reduction in the consistency index (Table 3). Overall, the effect of processing temperature is on the rate of attaining a given microstructure rather than differences in the final achieved microstructure for the formulation utilised in this study.

328 *Table 3. Properties of LGNs prepared at different structuring stage temperatures*

LGN	Viscosity gradient *b* to *d* (Pa s min s^{-1})	Peak viscosity value, *d,* (Pa s)	Time of peak viscosity, *d*, (s)	Final Viscosity value (Pa s)	Yield stress (Pa)	Consistency index, K (Pa s^n)	Flow index, n (-)
$LGN_{T=57}$	-	-	-	-	-	-	-
LGN_{ref}	6.1 x 10^{-2}	0.99± 0.03	1400	0.58 ± 0.02	108 ± 3	75.5	0.11
$LGN_{T=63}$	4.2 x 10^{-2}	0.92± 0.03	1650	0.57 ± 0.00	105 ± 5	75.0	0.13
$LGN_{T=67}$	2.4 x 10^{-2}	0.79± 0.11	2380	0.62 ± 0.03	104 ± 5	58.1	0.14

329

330 *3.1.3 Effects of vane speed on the formation of LGNs*

331 The effect of vane speed during the structuring stage on the formation of lamellar structured liquids
332 was explored for a range of shear rates of 50 $s^{-1,}$ 200 s^{-1}, 400 s^{-1}, and, 600 s^{-1}, respectively. The
333 temperature and time for the structuring stage were maintained at the reference conditions of 60°C
334 and 30 min. The viscosity profiles for these samples are given in Figure 5. To be able to directly
335 compare samples which have been prepared at different rotation speeds and therefore different
336 effective shear rates, it was necessary to transform the plots to show the apparent viscosity at the
337 reference shear rate of 200 s^{-1}. This was achieved using the method outlined in Section 2.3.

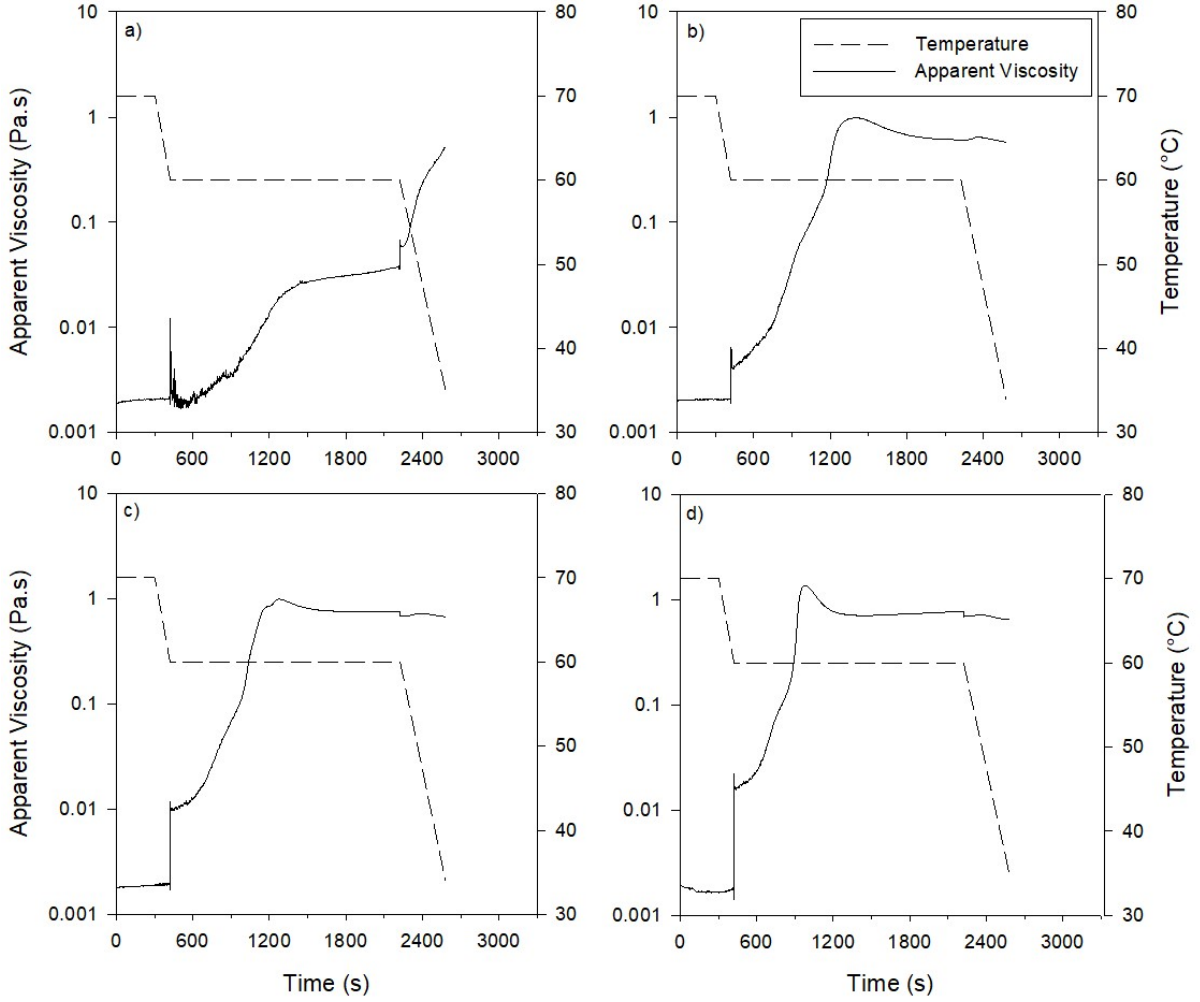

Figure 5. Viscosity-time plots for LGNs prepared at different structuring stage agitator speeds.
a) $LGN_{\gamma=50}$*, b)* LGN_{ref}*, c)* $LGN_{\gamma=400}$ *d)* $LGN_{\gamma=600}$
(dashed line = temperature profile; solid line = apparent viscosity)

338

Figure 5a shows the viscosity profile for $LGN_{\gamma=50}$ prepared at a shear rate of $50s^{-1}$. The viscosity-time plot at this lower vane speed does not follow the same trend as the reference sample (*Fig. 5b*), in terms of an initial jump in viscosity when the solid BTAC is added at point *b*, followed an increase in viscosity up to a maximum at *d*. For $LGN_{\gamma=50}$, after the BTAC addition at point *b*, the viscosity value slightly reduces to a value near 0.0001 Pa s at t = 420s, before increasing to 0.004 Pa s at t = 900s. The viscosity of the system then remains at approximately 0.005 Pa s for the remainder of the structuring stage. This suggests the vane speed was not sufficient to induce mixing in the system, thus a structure did not develop. Wunsch *et al.,* prepared a ternary system of cetostearyl alcohol, CTAC and water in a DSC pan by performing DSC on a mixture of solid cetostearyl alcohol and CTAC solution. They also found that when no shear was applied, the lamellar structure was not formed in the same way that it is under normal production methods, highlighting that shear also affects the ability of the system to form a lamellar gel phase (Wunsch, et al., 2015). The viscosity of the system did increase during the cooling stage, however this was ascribed to the re-solidification of FA which had not been incorporated in to any lamellar structure (Yamagata & Senna, 1999). Increasing the shear rate to 400 s^{-1} does not significantly ($p > 0.05$) affect the viscosity gradient between *b* and *d*, nor the time and value of the maximum viscosity (Table 4). Increasing the vane speed further to $600s^{-1}$ increases viscosity gradient significantly to 1.5 x 10^{-1} Pa $s.min^{-1}$, leading to a the maximum viscosity (1.37 Pa s) being achieved around 360s earlier than for LGN_{ref}. The effects of increasing the vane speed to $600s^{-1}$ were also evident from the rheological properties of the final product. The average yield stress did not increase significantly between the samples prepared at $200s^{-1}$ and $400s^{-1}$ (108±3 Pa and 110±18 Pa, respectively), however when the vane speed was increased to $600s^{-1}$, the yield stress of the final product was 136±10 Pa. When looking at the consistency index of the final LGNs, the samples follow a similar trend to yield stress, where the consistency index measured for LGN_{ref} and $LGN_{\gamma=400}$ were 75.5 Pa s^n and 79.3 Pa s^n respectively, and for $LGN_{\gamma=600}$ this increased to K = 112.7 Pa s^n. Neither the yield stress nor flow curve were able to be accurately measured for $LGN_{\gamma=50}$. Whilst there are no studies which have investigated the effect of energy input on the formation of lamellar gel networks, we can draw comparisons from emulsion formation and stability which has been more widely investigated. As expected, increasing the vane speed and thus the kinetic energy inputted to the

system did improve the mixing in the system, evidenced by the increased rate of viscosity build during stage *c*, which thus improved the final structure of the product, evidenced by higher yield stress and consistency index (Liu & McGrath, 2005).

371 *Table 4. Properties of LGNs prepared at different vane speeds*

LGN	Viscosity gradient *b* to *d* (Pa s min s^{-1})	Peak viscosity value, *d,* (Pa s)	Time of peak viscosity, *d*, (s)	Final Viscosity value (Pa s)	Yield stress (Pa)	Consistency index, K (Pa s^n)	Flow index, n (-)
$LGN_{\gamma=50}$	-	-	-	-	-	-	-
LGN_{ref}	6.1 x 10^{-2}	0.99± 0.03	1400	0.58 ± 0.02	108 ± 3	75.5	0.11
$LGN_{\gamma=400}$	6.9 x 10^{-2}	0.99± 0.31	1280	0.59 ± 0.08	110 ± 18	79.3	0.13
$LGN_{\gamma=600}$	2.4 x 10^{-2}	1.45± 0.02	1040	0.70 ± 0.04	136 ± 10	112.7	0.03

372

373 *3.1.4 Effects of processing time on the formation of LGNs*

374 The effects of varying time were investigated by varying the duration of the structuring stage for the
375 following times: 10 min, 20 min, 30 min, and 40 min. The temperature and vane speed were
376 maintained at the reference conditions, 60°C and 200s^{-1} respectively. Figure 6 shows the viscosity-
377 time plots for $LGN_{t=10,}$ $LGN_{t=20,}$ $LGN_{ref,}$ $LGN_{t=40}$.

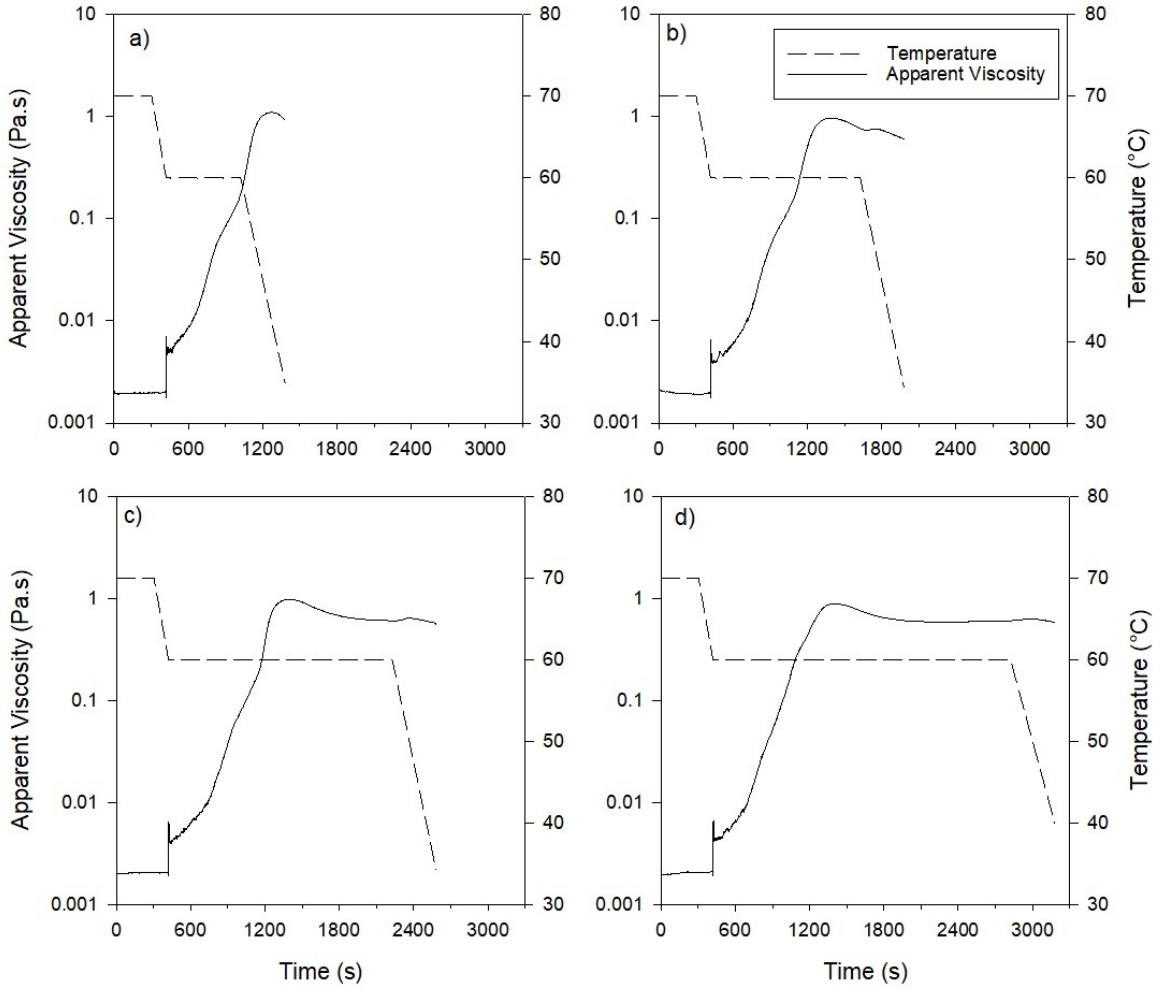

Figure 6. Viscosity-time plots for LGNs prepared at different structuring stage times. a) $LGN_{t=10}$, b) $LGN_{t=20}$ c) LGN_{ref} (30 minutes) d) $LGN_{t=40}$ (dashed line = temperature profile; solid line = apparent viscosity)

378

Figure 6a shows the viscosity time-plot for $LGN_{t=10}$ where a structuring stage time of 10 mins was used. Reducing the structuring stage to 10 mins had the largest effect on the viscosity during the formation of the incipient LGN. For most of the samples prepared at other conditions, the maximum viscosity occurs during the structuring stage. However, for $LGN_{t=10}$, the viscosity has not reached a steady-state at the end of the structuring stage as it does for the reference conditions, and instead the viscosity continues to increase to a maximum viscosity (1.18 Pa s) during the cooling stage at a temperature of 43°C. The maximum viscosity for $LGN_{t=10}$ is the second highest maximum viscosity achieved ($LGN_{\gamma=600,t=10}$ being the highest at 1.36 Pa s). This is reflected in the yield stress of the final product (139±8 Pa), which is the highest average yield stress value achieved. The higher yield stress and consistency of this sample suggest a well-connected and developed structure (Davies & Amin, 2020). Perhaps the reduced time at elevated temperatures provided less opportunity for the surfactant and FA to mix and form a lamellar liquid crystal, L_α, structure, followed by a transition to the lamellar gel phase accompanied by swelling, which is the predicted structure development (Wunsch, et al., 2015), and instead was able to immediately form a lamellar gel phase, L_β, at a temperature below the gel transition temperature during the cooling stage (Eccelston, 1997; Partal*, et al*., 2001). The oscillatory amplitude sweeps for the LGNs can be interpreted to provide further information about the microstructure (Figure 7). Youssry, *et al*. (2008) describe how a higher magnitude of the moduli can be attributed to stronger interactions between the flowing units – demonstrated by the slightly higher moduli for $LGN_{t=10}$ corresponding to a higher yield stress. Furthermore, the strain overshoot for the loss modulus (bump ~10% strain) is attributed to the formation of an intermediate structure which can resist strain up to a critical point (seen for LGN_{ref}). In this case, it is likely that MLVs are providing resistance to the strain. For $LGN_{t=10}$, the strain overshoot is absent, which suggests the lamellar phase is likely in a more swollen, planar state than LGN_{ref} which is more likely to have a higher proportion of MLVs present (Hyun, et al., 2002).

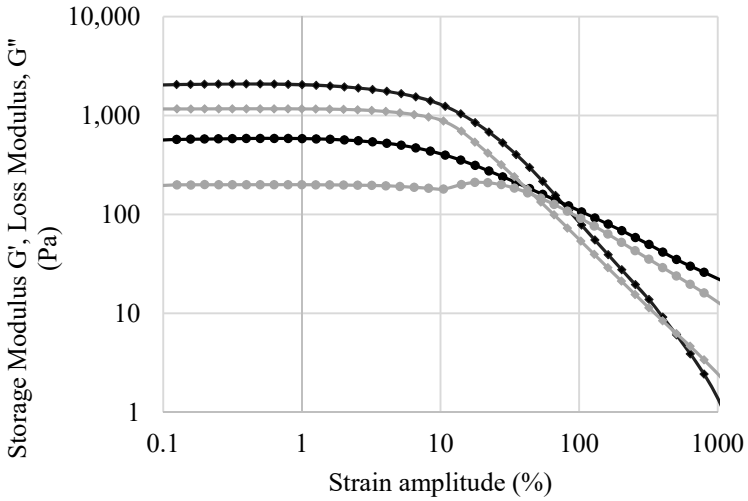

Figure 7. Oscillation amplitude strain sweep for LGN_{ref} and $LGN_{t=10}$ (grey = LGN_{ref}; black = $LGN_{t=10}$; diamond = G'; circle = G'')

403

404

405

406 Figure 6b shows the viscosity time plot for $LGN_{t=20.}$ For this processing time (20 mins), the viscosity
407 initially follows the same profile as samples prepared for longer times. The value of and time taken to
408 achieve the maximum viscosity are comparable to the sample prepared at the reference conditions
409 (Table 5). After point *d*, the reduced structuring stage time results in a reduction of the time from *d* to
410 *e* , the beginning of the cooling stage. This is beneficial from a processing perspective, as the system
411 is in steady state for this duration, so it is possible to reduce processing time without affecting product
412 structure and quality. The yield stress value measured for $LGN_{t=20}$ (108±13 Pa) is comparable to the
413 yield stress of LGN_{ref} and $LGN_{t=40}$ (Table 5), which further suggests that the majority of the structure
414 formation occurs before point *d*, and any additional mixing has little effect on the structure. The
415 variability in the yield stress values were slightly higher for $LGN_{t=20}$, which can be attributed to the
416 proximity of the end of the 20 minute structuring time to the typical time of the maximum viscosity
417 occurring (~1400 s). Figure 6c shows the viscosity time plot for LGN_{ref}, where a processing time of
418 30 min was used. Increasing the structuring stage time above the reference conditions to 40 min

(figure 6d) only increases the time between the peak viscosity at point *d* and the start of the cooling stage, *e,* where the viscosity of the system is not changing much as a function of time. This suggests that the structure of the system is also not changing, thus this increase in processing time is not conducive to improving the structuring of the incipient LGN. This is substantiated by the comparable time and value of the peak viscosity to the reference conditions (Table 5).

Table 5. Properties of LGNs prepared at different processing times

LGN	Viscosity gradient *b* to *d* (Pa s min s^{-1})	Peak viscosity value, *d,* (Pa s)	Time of peak viscosity, *d*, (s)	Final Viscosity value (Pa s)	Yield stress (Pa)	Consistency index, K (Pa s^n)	Flow index, n (-)
$LGN_{t=10}$	7.9 x 10^{-2}	1.18± 0.06	1040	0.93 ± 0.12	139 ± 8	44.3	0.21
$LGN_{t=20}$	5.9 x 10^{-2}	0.99± 0.07	1324	0.56 ± 0.04	101 ± 8	66.8	0.21
LGN_{ref}	6.1 x 10^{-2}	0.99± 0.03	1400	0.58 ± 0.02	108 ± 3	75.5	0.11
$LGN_{t=40}$	5.4 x 10^{-2}	0.95± 0.07	1400	0.59 ± 0.05	111 ± 11	88.5	0.06

As the greatest difference in microstructure formation and final product characteristics were observed from reducing the processing time and increasing the vane speed, it was decided to further investigate these characteristics by altering both conditions simultaneously. The conditions which were investigated were: a vane speed of 400s^{-1}, processing time of 20 minutes ($LGN_{\gamma=400,t=20}$) and a vane speed of 600s^{-1}, processing time of 10 minutes ($LGN_{\gamma=600,t=10}$). The samples were then compared against those prepared at the same shear rate, and reference processing time, and alternatively at the reference shear rate, and same processing time, to fully understand where the changes to the viscosity profile appear.

Figure 8 shows the viscosity profiles for $LGN_{\gamma=600,t=10}$, $LGN_{\gamma=600}$ and $LGN_{t=10}$. The samples prepared at the same shear rate ($LGN_{\gamma=600,t=10}$ and $LGN_{\gamma=600}$) initially follow a very similar profile, with peak *d* occurring at 1.37 Pa s, 980s for $LGN_{\gamma=600}$ and 1.40, 1020 Pa s for $LGN_{\gamma=600,t=10}$. The differences in the viscosity profile appear after the peak viscosity, *d*, in which the steady-state region is drastically

reduced, and begins at the beginning of the cooling stage, *e*. Comparing the samples prepared at the same time but different shear rates, it is easy to see that increasing the shear rate to $600s^{-1}$ increases the apparent viscosity from point *b* where the BTAC surfactant is added and the maximum viscosity value occurs earlier in the process, as previously discussed *(c.f. Fig.5)*.

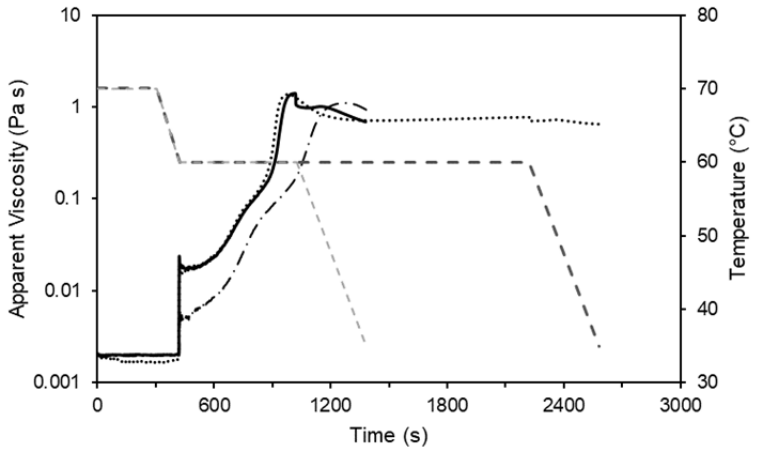

Figure 8. Viscosity-time plots for LGNs prepared at different times and agitator speeds (apparent viscosities: black solid line = $LGN_{\gamma=600,t=10}$, black dotted line = $LGN_{\gamma=600}$, black dot and dash line = $LGN_{t=10}$) (temperature profiles: dark grey dash line = 30 minute structuring stage ($LGN_{t=600}$), light grey dash line = 10 minute structuring stage ($LGN_{\gamma=600,t=10}$; $LGN_{t=10}$))

Interestingly when looking at the final properties of the LGNs, combining the reduced processing time with the higher shear rate does not produce a LGN with a higher yield stress than each condition individually. The yield stress for $LGN_{\gamma=600,t=10}$ is 125 Pa, compared to 136 Pa for $LGN_{\gamma=600}$ and 139 Pa for $LGN_{t=10}$. This could indicate that the vane speed is perhaps too high for short durations, and the effects of increased variability and fluctuations which often come with excessive mixing needs to be diminished by an increased processing time.

For $LGN_{\gamma=400,t=20}$, it was found that increasing the shear rate to $400s^{-1}$ and reducing the processing time to 20 min gave a profile which is initially similar to $LGN_{\gamma=400}$, with comparable times and values for the peak viscosity, *d*. However, for $LGN_{\gamma=400,t=20,}$ the time between *d* and the start of the cooling phase

452 *e* is obviously reduced and shows the same trend as $LGN_{t=20,}$ *i.e.,* a reduction in the duration of the
453 steady state phase. Comparing $LGN_{\gamma=400;t=20}$ to $LGN_{t=20,}$ which was prepared at the reference shear rate
454 ($200s^{-1}$), the rate of viscosity increase is higher for $LGN_{\gamma=400;t=20}$ (8.22×10^{-2} Pa $s.min^{-1}$) from *b* to *d*,
455 compared to 5.88×10^{-2} Pa $s.min^{-1}$. The value of the maximum viscosity also increased as a function
456 of vane speed. The effects of increasing vane speed and reducing processing time increased the final
457 yield stress of $LGN_{\gamma=400,t=20}$ (129±6 Pa), higher than for both $LGN_{t=20}$ (*c.f. Table 5*) and $LGN_{\gamma=400}$ *(c.f.*
458 *Table 4)* .

459

460 *3.2 Effects of processing conditions on power consumption*

461 As well as investigating the effects of varying process conditions on the rheological properties
462 of the final LGN, it was also important to determine the process requirements for each set of
463 conditions. **Error! Reference source not found.**a shows a plot of the total mixing energy and energy
464 input until the maximum viscosity was achieved as a function of temperature. At 57°C, there was no
465 maximum viscosity so there is no value for this point. Above 60°C, as the temperature increases, the
466 total mixing energy required reduces, as the system spends a longer portion of the process at a
467 reduced viscosity (*cf.,* Fig 4). However, the power required to maintain the temperature of the system
468 has not been considered in this work. This also explains why the energy required to achieve the
469 maximum viscosity is higher for $LGN_{T=67}$ as the maximum viscosity is achieved ~1000s later than for
470 LGN_{ref}. **Error! Reference source not found.**b shows energy requirements as a function of vane
471 speed (s^{-1}). The total energy input increases linearly as the vane speed is increased, whilst the energy
472 required to achieve the maximum viscosity does not increase with vane speed; it is comparable
473 amongst all the different speeds, 1.18 J/g for LGN_{ref}, 1.18 J/g for $LGN_{\gamma=400}$ and 1.63 J/g for $LGN_{\gamma=600}$.
474 From **Error! Reference source not found.**c, it can be seen that total energy input increases in an
475 exponential manner as a function of structuring stage time. However, the energy required to achieve
476 maximum viscosity is again comparable for all structuring times (1.18 J/g), which is logical as the
477 maximum viscosity occurs at a similar time for samples prepared at the same vane speed. For
478 $LGN_{\gamma=400,t=20}$, the energy input required to achieve the maximum viscosity was 1.18 J/g – again

comparable to most of the other samples. However, for $LGN_{\gamma=600,t=10}$, the energy input required to achieve maximum viscosity was 2.29 J/g. Out of the samples with the highest yield stress, $LGN_{t=10}$ and $LGN_{t=600}$, $LGN_{t=10}$ had the lowest energy requirements. Reducing the processing time offers the most obvious option for reducing power consumption, whilst maintaining a high yield stress. This said, the total energy input for $LGN_{\gamma=600,t=10}$ (2.29 J/g) was one of the lowest which still produced a comparatively high yield stress.

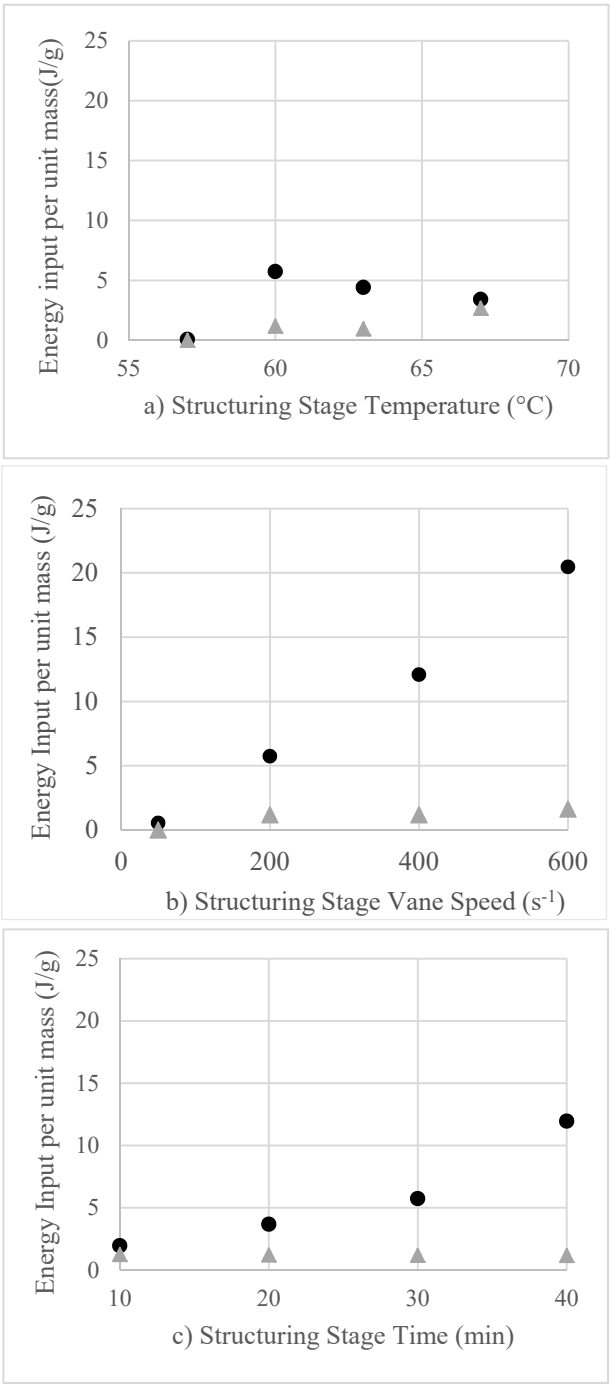

Figure 9. Total energy input per unit mass for different LGN processing conditions.
a) different structuring stage temperatures
b) different structuring stage vane speeds
c) different structuring stage times
(black circle = total energy input; grey triangle = energy input to maximum viscosity value.)

485

486
487

4 CONCLUSIONS

The structure formation of a lamellar gel network system comprised of water, cetostearyl alcohol and BTAC has been followed through the use of a rheological mapping approach. A four-bladed vane and cup geometry rotational rheometer was utilised to follow the viscosity and power requirements of the system as a function of time. This work presents an insight into the kinetics of lamellar structure formation during processing, which has not been widely explored yet. Most other studies which have considered process conditions have only been able to focus on the properties of the sample after preparation. It was seen that the system typically followed a profile in which, after surfactant addition, the viscosity increased at a rate of 6.0 x $^{10-2}$ Pa s.min^{-1} up to a maximum value which occurred around 1400s (for LGN_{ref}). There was a slight secondary peak that occurred during the cooling stage, which was attributed to the swelling of the gel phase. The effects of process history on the final rheological characteristics were determined through traditional oscillatory and rotational rheometry techniques. The results provide information about how process conditions can be varied to improve final product quality, as well as reduce power consumption. An increase in temperature lead to an increased time to achieve a maximum viscosity but did not have a significant effect on the final yield stress of the samples. Variation of the vane speed proved the importance of shearing when producing a lamellar structure. At the lowest vane speed, a structure was not formed and the viscosity profile did not follow the anticipated pattern demonstrated for the reference conditions. Increasing the vane speed to the maximum speed tested here ($600s^{-1}$) led to an increase in the yield stress and consistency index of the final LGN, as well as an increase in the maximum viscosity seen during processing and a reduction in the time taken to achieve the maximum viscosity. However, the power requirements increased linearly with increased vane speed, meaning the total energy input for this sample was three times that for the reference conditions. Finally, it can be seen that increasing the structuring stage time past 30 minutes had minimal effect on the structure of the system, and only increased the steady-state phase of the process. Reducing the structuring stage time to 20 min provided the same yield stress, but reduced the power requirements. Reducing the time further to 10 min further increased the yield stress, and this is thought to be associated with the lamellar gel phase forming at a cooler temperature rather than first forming a lamellar liquid crystal and then

transforming to gel when the system cools below the gel transition temperature. In the future it would be beneficial to investigate different formulations, such as different concentrations of the same components, or other surfactants to see if changing processing conditions has the same effect across formulations. Additionally, another aspect which would be interesting to explore is the use of a close clearance vane such as anchor or helical ribbon which would more commonly be used in larger scale processes to determine the suitability of this technique for scale-up considerations.

Acknowledgements

The authors would like to acknowledge Dr. Andre Botha and Dr. Cesar Mendoza at Unilever Research & Development, Port Sunlight, UK for their helpful discussions regarding this study, and Ellie Farrar at University of Birmingham for assistance with experimental work. Authors acknowledge financial support received from the Centre for Doctoral Training in Formulation Engineering (EPSRC grant no.EP/S023070.1).

530 **REFERENCES**

531 Ahmadi, D. et al., 2020. The Influence of Co-Surfactants on Lamellar Liquid Crystal Structures
532 Formed in Creams. *Pharmaceutics,* 12(864).

533 Ait-Kadi, A. et al., 2002. Quantitative Analysis of Mixer-Type Rheometers using the Couette
534 Analogy. *The Canadian Journal of Chemical Engineering,* Volume 80.

535 Awad, T. S., Johnson, E. S., Bureiko, A. & Olsson, U., 2011. Colloidal Structure and Phsyical
536 Properties of Gel Networks Containing Anionic Surfactant and Fatty Alcohol Mixture. *Journal of*
537 *Dispersion Science and Technology,* 32(6).

538 Ballmann, C. & Mueller, B., 2008. Stabilizing Effect of Cetostearyl Alcohol and Glycerylmonstearate
539 as Co-emulsifiers on Hydrocarbon-free O/W Glyceride Creams. *Pharmaceutical Development and*
540 *Technology,* 13(5), pp. 433-445.

541 Bousmina, M., Ait-Kadi, A. & Faisant, J., 1999. Determination of shear rate and viscosity from batch
542 mixer data. *Journal of Rheology,* 43(415).

543 Chavez-Montes, B., Choplin, L. & Schaer, E., 2003. Rheo-reactor for studying the processing and
544 formulation effects on structural and rheological properties of ice cream mix, aerated mix and ice
545 cream. *Polymer International,* Volume 52, pp. 572-575.

546 Choplin, L. & Marchal, P., 2010. Mixer-Type Rheometry. In: *Rheology.* s.l.:EOLSS Publications.

547 Choplin, L., Torandell, S. & Servoin, J., 1998. In situ rheological monitoring in semi-batch
548 emulsification process for cosmetic lotion production. *The Canadian Journal of Chemical*
549 *Engineering,* Volume 76.

550 Clairant Corporation, 2018. *Genamin BTLF Safety Data Sheet.* Charlotte, NC: Clairant Corporation.

551 Colafemmina, G. et al., 2020. The cooling process effect on the bilayer phase state of the
552 CTAC/cetearyl alcohol/water surfactant gel. *Colloids and Surfaces A: Physicochemical and*
553 *Engineering Aspects,* Volume 587.

554 Datta, A. et al., 2020. Characterizing the rheology, slip, and velocity profiles of lamellar gel networks.
555 *Journal of Rheology,* 64(851).

556 Davies, A. & Amin, S., 2020. Microstructure design of CTAC:FA and BTAC:FA lamellar gels for
557 optimized rheological performance utilizing automated formulation platform. *International Journal of*
558 *Cosmetic Science,* Volume 42, pp. 259-269.

559 Eccelston, G. M., 1997. Functions of mixed emulsifiers and emulsifying waxes in dermarological
560 lotions and creams. *Colloids and Surfaces A: Physicochemical and Engineering Aspects,* Volume 123,
561 pp. 169-182.

562 Fairhurst, D. J., Baker, M. E., Shaw, N. & Egelhaaf, S. U., 2008. Swelling and shrinking kinetics of a
563 lamellar gel phase. *Applied Physics Letters,* Volume 92.

564 Flanagan, M., 2013. *Process.* Global, Patent No. WO14016350 A1.

565 Franco, J. et al., 2005. Mixing rheometry for studying the manufacture of lubricating greases.
566 *Chemical Engineering Science,* 60(8-9), pp. 2409-2418.

567 Fukushima, S. & Yamaguchi, M., 1983. The effect of cetostearyl alcohol in cosmetic emulsions.
568 *Cosmetics & Toiletries,* Volume 98, pp. 89-102.

569 Gaini, C. et al., 2006. The dissolution behaviour of native phosphocaseinate as a function of
570 concentration and temperature using a rheological approach. *International Dairy Journal,* 16(12), pp.
571 1427-1434.

572 Gentile, L. et al., 2014. Dynamic Phase Diagram of a Nonionic Surfactant Lamellar Phase. *The*
573 *Journal of Physical Chemistry B,* Volume 118, pp. 3622-3629.

574 Gentile, L., Rossi, C. O. & Olsson, U., 2012. Rheological and rheo-SALS investigation of the multi-
575 lamellar vesicle formation in the C12E3/D2o system. *Journal of Colloid and Interface Science,*
576 367(1), pp. 537-539.

Grollier, J. F. & Richoux, I., 1993. *COSMETIC PREPARATION FOR THE CARE OF THE HAIR AND USE OF THE SAID COMPOSITION.* US, Patent No. US5246693.

Hyun, K., Kim, S. H., Ahn, K. H. & Lee, S. J., 2002. Large amplitude oscillatory shear as a way to claassify the complex fluids. *Journal of non-Newtonian Fluid Mechanics,* Volume 107, pp. 51-65.

Ito, M., Kosaka, Y., Kawabata, Y. & Kato, T., 2011. Transition process from the lamellar to the onion state with increasing temperature under shear flow in a nonionic surfactant/water system studied by Rheo-SAXS. *Langmuir,* 27(12), pp. 7400-7409.

Iwata, K. & Aramaki, K., 2003. Effect of the behenyl trimethyl ammonium counterion on the lamellar gel property. *IFSCC Magazine*, Volume 16, pp. 249-254.

Iwata, T., 2017. Chapter 25 - Lamellar Gel Network. In: K. Sakamoto, R. Y. Lochhead, H. I. Maibach & Y. Yamashita, eds. *Cosmetic Science and Technology.* Kobe: Elsevier, pp. 415-447.

Iwata, T. & Aramaki, K., 2013. Effect of the Behenyl Trimethyl Ammonium Counterion on the Lamellar Gel Property. *International Federation of Societies of Cosmetic Chemists*, Volume 4, pp. 249-254.

Junginger, H., 1984. Colloidal Structures of O/W Creams. *Pharmaceutisch Weekblad Scientific Edition,* Volume 6, pp. 141-149.

Liu, E.-H. & McGrath, K. M., 2005. Emulsion microstructure and energy input, roles in emulsion stability. *Colloids and Surfaces A: Physicochemical and Engineering Aspects,* 262(1-3), pp. 101-112.

Metzner, A. & Otto, R., 1957. Agitation of non-Newtonian fluids. *AIChE Journal,* 3(1).

Nakama, Y., 2017. Chapter 15 - Surfactants. In: *Cosmetic Science and Technology: Theoretical Principles and Applications.* Kanagawa, Japan: Kishi Kasei Co., Ltd., pp. 231-244.

Nakarapanich, J. et al., 2001. Rheological properties and structures of cationic surfactants and fatty alcohol emulsions: effect of surfactant chain length and concentration. *Colloid and Polymer Science,* Volume 279, pp. 671-677.

Partal, P. et al., 2001. Rheology and Microstructural Transitions in the Lamellar Phase of a Cationic Surfactant. *Langmuir,* Volume 17, pp. 1331-1337.

Rabia, A. et al., 2014. Optimization of the vane geometry. *Rheologica Acta,* Volume 53, pp. 357-371.

Ribiero, H., Morais, J. & Eccleston, G., 2004. Structure and rheology of semisolid o/w creams containing cetyl alcohol/non-ionic surfactant mixed emulsifier and different polymers. *International Journal of Cosmetic Science,* Volume 26, pp. 47-59.

Venkateswaran, A., Yang, J. Z. & Toshiyuki, O., 2009. *HAIR CONDITIONING COMPOSITION CONTAINING BEHENYL TRIMETHYL AMMONIUM CHLORIDE, AND HAVING HIGHER YIELD POINT.* US, Patent No. US2009324527.

Wunsch, K. et al., 2015. Effect of surfactant on structure thermal behaviour of cetyl stearyl alcohols. *Journal of Thermal Analysis and Calorimetry,* Volume 123, pp. 1411-1417.

Yamagata, Y. & Senna, M., 1999. Change in Viscoelastic Behaviors Due to Phase Transition of the Assembly Comprising Cetyltrimethylammonium Chloride/Cetyl Alcohol/Water. *Langmuir,* 15(13), pp. 4388-4391.

Yang, J., 2017. Chapter 36 - Hair Care Cosmetics. In: K. Sakamoto, R. Y. Lochhead, H. I. Maibach & Y. Yamashita, eds. *Cosmetic Science and Technology: Theoretical Principles and Applications.* Kobe: Elsevier, pp. 601-615.

Youssry, M., Coppola, L., Nicotera, I. & Morán, C., 2008. Swollen and collapsed lyotropic lamellar rheology. *Journal of Colloids and Interface Science,* 321(2), pp. 459-467.

Zhong, Y. J. & Toshiyuki, O., 2009. *Hair Conditioning Composition Having Higher Yield Point And Higher Conversion Rate Of Fatty Compound To Gel Matrix.* European Patent Office, Patent No. EP2460508 A1.

~~*er Conversion Rate Of Fatty Compound To Gel Matrix.* European Patent Office, Patent No. EP2460508 A1.~~

625

626

627

628

629

630

631

632

633

634

635

636

637

638